Nanoscale control of Si nanoparticles within a 2D hexagonal array embedded in SiO2 thin films

Celia Castro, Gérard Benassayag, Béatrice Pécassou, Andrea Andreozzi, Gabriele Seguini, Michele Perego, Sylvie Schamm-Chardon

Nanoscale control of Si nanoparticles within a 2D hexagonal array embedded in SiO2 thin films

Celia Castro[a,], Gérard BenAssayag[a], Béatrice Pecassou[a], Andrea Andreozzi[b], Gabriele Seguini[b], Michele Perego[b] and Sylvie Schamm-Chardon[a]***

[a] MEM group, CEMES-CNRS UPR 8011 et Université de Toulouse, 29 rue Jeanne Marvig, 31055 Toulouse, France

[b] Laboratorio MDM, IMM-CNR Via C Olivetti 2, 20864 Agrate Brianza (MB), Italy

* Corresponding author e-mail: sylvie.schammchardon@cemes.fr

** now at Normandie Univ, UNIROUEN, INSA Rouen, CNRS, Groupe de Physique des Matériaux, 76000 Rouen, France

Abstract

In this work, we investigate the ability to control Si nanoparticles (NPs) spatially arranged in a hexagonal network of 20 nm wide nanovolumes at controlled depth within SiO_2 thin films. To achieve this goal an unconventional lithographic technique was implemented based on a bottom-up approach, that is fully compatible with the existing semiconductor technology. The method combines ultra-low energy ion beam synthesis (ULE-IBS) with nanostructured block-copolymer (BCP) thin films that are self-assembled on the SiO_2 substrates to form a nanoporous template with hexagonally packed pores. A systematic analytical investigation using time of flight-secondary ion mass spectroscopy (ToF-SIMS) and low-loss energy filtered transmission electron microscopy (EFTEM) demonstrates that by adjusting few fabrication parameters, it is possible to narrow the size distribution of the NPs and to control the number of nanoparticles per nanovolume. Experimental results are critically discussed on the basis of literature data, providing a description of the mechanism involved in the formation of Si NPs.

KEYWORDS: silicon nanoparticles, nanocrystals, PS-b-PMMA, Block-Copolymer, Ultra-Low Energy Ion Implantation Synthesis, Energy Filtered TEM, TOF-SIMS

1. Introduction

Because of their broad spectrum of potential functionalities, layers of buried nanoparticles made of organized individual nanodots or nanowires at nanoscale are anticipated to be the next generation of high performance electronic devices [1–3]. Innovative nanofabrication tools for readily positioning in three dimensions and for interfacing these single nanostructures in functional devices are essential to overcome the well-known current downscaling limitations of conventional photolithography [1–3]. Promising results are expected by combining various nanopatterning approaches (lithography, stencil mask, reactive ion etching…) and nanoparticle synthesis (chemical vapor deposition, atomic layer deposition, e-beam evaporation, ion implantation…) [4,5]. Si nanoparticles (NPs) embedded in a dielectric matrix are exemplary structures extensively studied [6–12] for their integration in active devices for nanoelectronics, optoelectronics and photovoltaics [13–16]. These model structures are therefore good candidates to demonstrate the performances of new fabrication tools with a control over the nanometric size of the NPs.

Among nanoparticles synthesis techniques, routinely used in semiconductor industry, ion beam synthesis (IBS) is characterized by its versatility for the direct fabrication of embedded nanostructures [6,7,17]. Playing with ions of ultra-low energy (ULE) at high fluence, and with post-treatment annealing conditions (duration, temperature, and atmosphere), the size, density and depth distribution of Si NPs within silica thin films were easily manipulated [18,19].

Typically, with Si^+ implantation at 1 keV and a fluence of about 10^{16} ions/cm^2 into thin oxide layers followed by annealing around 1000 °C, two-dimensional (2D) arrays of Si NPs embedded few nanometers below the SiO_2 surface are formed [20].

Nanopatterning these systems with the purpose to control the positioning of individual NPs in the plane they form is very challenging. The coupling of ULE-IBS with standard stencil masks has shown strong limitations to provide submicronic patterns. Limitations in ion fluence control were suggested to come from charge screening effect due to ions accumulated inside the stencil and the non-direct contact with the underneath substrate [21].

A further downscaling option consists in the introduction of a nanopatterned polymeric mask in close contact with the underlying substrate. Top down approaches based on e-beam lithography or nanoimprint lithography have been demonstrates to be perfectly suitable for the fabrication of nanostructured polymeric templates with minimum feature size below 20 nm [22]. Alternative bottom up approaches based on block copolymer (BCP) self-assembly provide a viable solution to fabricate nanoporous templates that can be implemented as soft mask for subsequent additive or subtractive fabrication processes [23,24]. BCPs are promising candidates to overcome downscaling limitations of optical lithography and have emerged as low cost and compatible with microelectronic industries [2,25]. BCPs microphase separate and self-assemble into periodic nanostructures with periods between 10 and 100 nm [26]. After selective removing of one of the two components, these thin films are interesting soft mask for nanolithographic processes. In particular, the cylindrical and lamellar configurations are attractive structures for nanodots and nanowires synthesis [5,27]. Direct deposition of metal nanodots has been performed considering the BCP mask as nanopattern for deposition by lift-off processes. Another method consists to template the substrates by reactive ion etching through the BCP mask

[5,28,29]. In a previous work, we succeeded in combining ULE-IBS with a cylinder type nanoporous BCP mask composed of a polystyrene matrix [30]. The BCP mask is acting as a stencil without affecting significantly the NPs characteristics. A hexagonal array of nanovolumes composed of few Si NPs is then synthesized.

This approach was the first successful step towards our main goal, which is to generate and interface nano-objects on large areas with extremely high accuracy in terms of position and reproducibility. The purposes of this paper are first to study the mechanism of the implantation process along the different steps encountered during the combination of BCP with ULE-IBS and second, to determine how the characteristics of Si NPs (size, number per nanovolume) are modified changing the synthesis parameters such as fluence and annealing treatment. The final aim being to identify the present limitations of our nanofabrication approach and foresee its future developments. The systems investigated have nanoscale dimensions over micrometric areas. Thus, our strategy to investigate with reliability these multiscale systems was to combine statistical analysis using Time-of-Flight Secondary Ion Mass Spectrometry (TOF-SIMS) with highly localized Energy Filtered Transmission Electron Microscopy (EFTEM).

2. Experimental details

2.1. Synthesis of Block Copolymer mask.

The complete protocol for the fabrication of the nanoporous polystyrene (PS) mask has been previously reported [27,29,30]. Briefly, the self-assembled BCP templates are formed on top of 16 nm thick SiO_2 films thermally grown on (100) oriented silicon wafers. First, the substrates are cleaned (Piranha solution, at 80°C for 60 min) and properly neutralized by grafting a OH-terminated poly(styrene-*random*-methyl methacrylate) (PS-*r*-PMMA) random copolymer on the SiO_2 substrate. The selected PS-*r*-PMMA has molecular weight M_n = 11400 g/mol and a styrene

fraction f = 0.58. The ungrafted chains were removed with a 300 s sonication step in a toluene bath. Then the asymmetric polystyrene-*block*-poly(methyl methacrylate) (PS-*b*-PMMA) BCP (M_n = 67100 g/mol, f = 0.71) is spun on the neutralized substrates. The samples are annealed in a conventional furnace (190°C, 2h, 3.10^{-2}mbar) to promote the self-organization of the PS-*b*-PMMA BCP into hexagonal arrangement of PMMA cylinders embedded in a PS matrix and perpendicularly oriented with respect to the substrate. Finally, in order to form the porous mask, the PMMA blocks are selectively removed (UV exposure, acetic acid bath) and PS-r-PMMA at the bottom of the pores is etched by an oxygen plasma treatment. The resulting nanoporous PS mask is a thin film of 21 ± 4 nm in thickness with pores distance L_0 = 33.1 ± 0.3 nm and mean pore diameter d = 17.3 ± 0.4 nm. These data correspond to an exposed area through the pores of the mask that is equivalent to 25% of the total area of the underlying substrate. In addition some test samples were prepared using a different PS-*r*-PMMA random copolymer (M_n = 13500 and f = 0.62). As already reported in the literature [27], when using this random copolymer to neutralize the substrate, the final nanoporous templates exhibit different characteristic dimensions. The thicker random copolymer brush layer that is used to neutralize the substrate requires longer etching processes to remove the residual random copolymer from the bottom of the pores after the selective removal of the PMMA cylinders. Actually, the prolonged O_2 plasma treatment determines a progressive enlargement of the pores due to lateral etching of the PS template. In particular, after the complete opening of the pore, the average pore diameter was determined to be d = 20.7 ± 0.6 nm, while no variation of the center-to-center distance L_0 between the nearest pores was observed. These data correspond to an exposed area through the pores of the mask that is equivalent to 37% of the total area of the substrate.

2.2. Nanoparticles fabrication by ULE-IBS and annealing

Si^+ implantation (1keV, 0.50 $x10^{16}$, 0.75$x10^{16}$ or 1$x10^{16}$ Si^+ ions/cm^2) is then performed through the mask but also on bare samples (without BCP) used as reference. Phase separation of the implanted Si from the oxide matrix to form Si NPs is obtained by high thermal annealing at 1050°C under N_2 during 30 min or 90 min. This is done after removal of the BCP by mean of piranha solution. More details about the BCP mask preparation and removal as well as on the ion implantation process can be found in [20,27,30]. The 3 mains steps of the process are shown in figure 1.

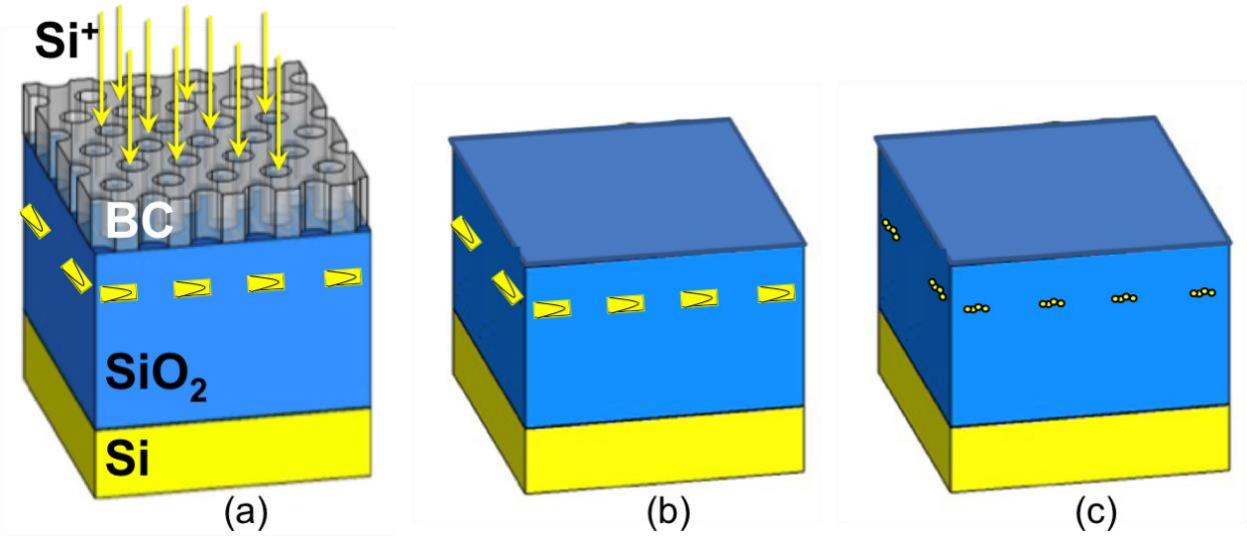

Figure 1. Schematic representation of the BCP and ULE-IBS combination process: (a) implantation of Si^+ ions in the SiO_2 layer through the BCP and formation of local Si supersaturation (Si-implanted profiles), (b) removal of the BCP and (c) formed Si NPs after the thermal treatment.

2.3. Multiscale characterization of the nanoparticles

TOF-SIMS profiles were acquired on an IONTOF IV system operating in negative polarity. Sputtering was accomplished by Cs^+ ions at 1 keV, rastering over a 200 x 200 m^2 area. The analysis was performed by using Ga^+ ions operating at 25 keV, rastering over a 50 x 50 m^2 area.

TOF-SIMS data were normalized with the value of the $^{30}Si^-$ signal detected in bulk silicon in order to remove variations of the signals intensity due to fluctuations of the Ga current.

Energy Filtered TEM (EFTEM) was performed on a field emission aberration-corrected microscope (FEI Tecnai^{TM} F20) operating at 200 kV and equipped with an imaging filter (TRIDIEM Gatan). EFTEM images were formed from selected electrons that loose energy corresponding to the plasmon energy of Si, i.e 17 eV (± 2 eV) when interacting with the sample [31]. TEM specimens were prepared for cross-section and plan-view observations using the standard procedure involving mechanical polishing and Ar^+ ion milling. The TEM lamellae were thin enough to see the NPs with sufficient contrast, i.e. 10 nm. The electron dose and the duration of acquisition were controlled in order to avoid irradiation effects as discussed in [28].

3. Results

3.1. The set of studied samples

For the purpose of this study, a set of 18 samples has been prepared with different fabrication parameters as described in table 1. The name of the samples accounts for these fabrication parameters, i.e. the sample B25_050_30 has been prepared with a BCP-masked substrate (B), an exposed area (open pore surface fraction) of 25 %, a $0.5x10^{16}$ Si^+ ions/cm^2 fluence (050) and a 30-minute annealing duration (30). The choice of the parameters in Table 1 allows comparing flat (F) surface and BCP (B) patterned surfaces for different fluences and different annealing durations. Two BCP were used with a pore/surface ratio that corresponds to an exposed area equivalent to 25% or 37% of the total area of the substrate. A first set of samples (10 first samples of table 1) was dedicated to TOF-SIMS analyzes to compare fluence and BCP induced modifications. A second set of samples (8 last samples of table 1) was dedicated to EFTEM

analyzes. This set, annealed at 1050 °C under N_2 after implantation, explores three Si^+ fluences and two annealing durations, particularly for the masked samples with a 25% exposed area.

Sample	Surface Patterning (nm)	Implantation Fluence (x 10^{16} Si^+ ions/cm²)	Annealing Duration (min)
F_030	FLAT	0.30	-
F_050	FLAT	0.50	-
F_075	FLAT	0.75	-
F_100	FLAT	1.00	-
F_150	FLAT	1.50	-
B25_050	BCP 25%	0.50	-
B25_075	BCP 25%	0.75	-
B25_100	BCP 25%	1.00	-
B37_075	BCP 37%	0.75	-
B37_100	BCP 37%	1.00	-
F_050_30	FLAT	0.50	30
F_075_30	FLAT	0.75	30
F_100_30	FLAT	1.00	30
B25_050_30	BCP 25%	0.50	30
B25_075_30	BCP 25%	0.75	30
B25_100_30	BCP 25%	1.00	30
B25_075_90	BCP 25%	0.75	90
B25_100_90	BCP 25%	1.00	90

Table 1. List of the studied samples with their fabrication parameters; ULE-IBS beam energy is 1 keV.

3.2. Effect of the mask on the implantation process

In order to follow the way Si is incorporated in the silica matrix just after implantation and after BCP removal, ToF-SIMS compositional depth profiles were systematically registered for the masked samples after the implantation with Si^+ ions at 1 keV and different fluences. The ToF-

SIMS profiles of the samples before and after the removal of the BCP template are reported in figure 2 and figure 3 respectively.

The analysis of the raw data was performed using a full spectrum approach that allows clearly identifying the different matrices and discriminating the excess of silicon introduced in the SiO_2 film during implantation by means of secondary cluster ion signals [32]. In particular the C_n^- signals ($1 \leq n \leq 5$) are representative of the nano-porous BCP layer, the SiO_n^- ($1 \leq n \leq 4$) signals identify the SiO_2 film, while the Si_n^- signals ($1 \leq n \leq 6$) are used to single out the Si substrate and the Si excess [33,34]. For the sake of clarity only a limited number of representative SiO_n^- and Si_n^- signals is reported in figure 2 and figure 3.

It is worth to note that the depth resolution of the profiles depicted in figure 2 is limited by the porosity of the BCP template whose effect is a slight broadening of the profiles that is equivalent to the one observed in samples characterized by remarkable surface roughness. Despite this experimental constrain, it is possible to clearly discriminate in the profiles the different layers corresponding to the 21 nm thick PS film, the 16 nm thick SiO_2 and, finally, the Si substrate. It is worth to note that the depth calibration was performed assuming a constant sputter rate throughout the profiles and using a 16 nm thick SiO_2 as a reference sample to measure the sputter velocity and to perform the time-to-depth conversion [35]. This choice implies that the thickness of the SiO_2 film in the profiles of figure 2 is properly addressed while the thickness of the PS layer is underestimated. The main advantage of this choice is the possibility to easily compare the profiles of the SiO_2 layer in figure 2 with those reported in figure 3.

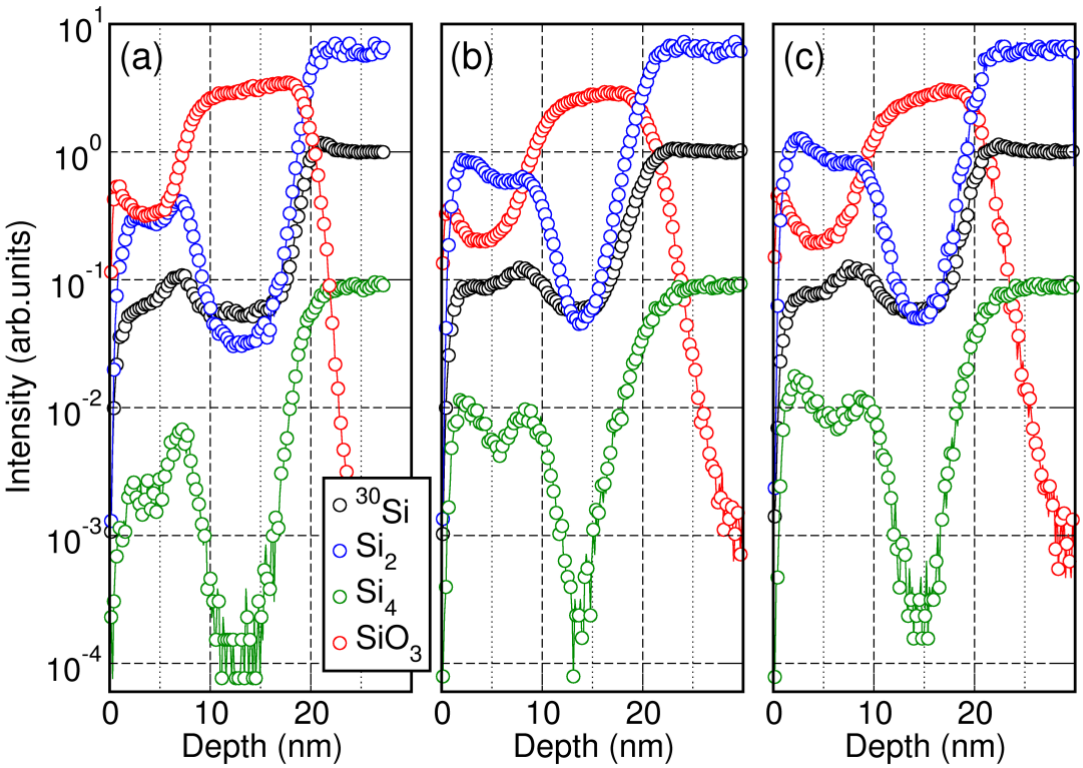

Figure 2. ToF-SIMS depth profiles of 16 nm thick SiO_2 films implanted through a nanoporous PS template with Si^+ ions at 1 keV with fluences $0.5x10^{16}$ (a), $0.75x10^{16}$ (b) and $1.0x10^{16}$ (c) ions/cm^2. The profiles were acquired just after the implantation step to investigate the effective trapping of Si in the PS mask.

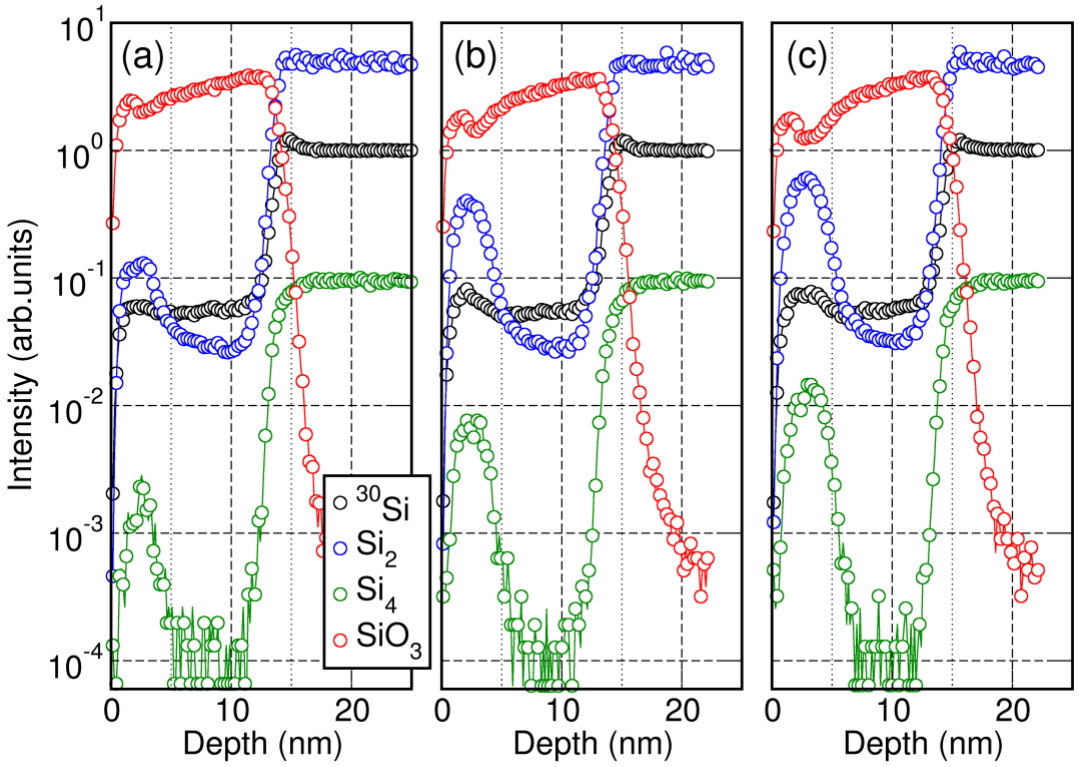

Figure 3. ToF-SIMS depth profiles of 16 nm thick SiO_2 films implanted through a nanoporous PS template with Si^+ ions at 1 keV with fluences $0.5x10^{16}$ (a), $0.75x10^{16}$ (b) and $1.0x10^{16}$ (c) ions/cm^2. The profiles were acquired after the removal of the PS template to investigate the effective trapping of Si in the SiO_2 substrate.

The analysis of the as implanted samples reveals that part of the Si^+ ions is effectively trapped in the PS template as expected. This is clearly visible in figure 2 where the Si_2^- and Si_4^- signals spot a systematic accumulation of silicon in the polymeric film. These Si_n^- profiles are characterized by two relative maxima; the one close to the surface is attributed to the Si atoms implanted in the PS matrix, the second one is mainly ascribed to an interface effect, i.e. to a variation of the secondary ion signal due to an artefact of the measurement occurring when profiling at the interface among two different matrices. Consequently this second peak is not representative of the depth distribution of silicon in the sample. This interface effect and the

limited depth resolution at the PS/SiO_2 interface do not allow clearly detecting the Si_n^- signal of the silicon implanted in the SiO_2 matrix. Nevertheless, the progressive increase of the Si_n^- relative maxima, close to the sample surface, well correlates with the increasing fluencies ($0.5x10^{16}$, $0.75x10^{16}$ and $1.0x10^{16}$ ions/cm^2) of the Si implants as clearly highlighted in figure 2(a), (b) and (c) respectively. Moreover these data qualitatively demonstrate that the thin PS films did not significantly deteriorate during ion implantation and successfully acted as a shadow mask stopping the Si^+ ions even at very high fluencies.

Figure 3 reports the ToF-SIMS depth profiles of the same samples after removal of the PS template by rinsing the sample in piranha solution for 40 min. No more evidence of the polymeric film is present in the profiles. After the removal of the PS template, we registered a significant increase in depth resolution. The depth profiles show the presence of well-defined Si_n^- relative maxima in the SiO_2 matrix. These signals are representative of the excess of silicon introduced in the SiO_2 film during ion implantation in agreement with our previous studies on similar systems [33,34]. The projected range of the implanted silicon is around 2.5 nm, in agreement with the values obtained in the reference samples prepared by implanting directly in the SiO_2 film without the nanoporous polymeric mask (data not shown). The intensity of the Si_n^- relative maxima progressively increased with the fluence, demonstrating the effective capability to modulate the amount of Si ions implanted in the SiO_2 matrix through the nanoporous template.

In order to get a better qualification of the implantation process throughout the polymeric template we integrated the Si_n^- signals in the region corresponding to the relative maxima. Figure 4 reports the corresponding integrated Si_2^- values as a function of implantation fluencies. This nanoporous polymeric template has average pore diameter $d = 17.3 \pm 0.4$ nm and the center-to-center distance $L_0 = 33.2 \pm 0.7$ nm. As previously discussed, considering the pore/surface ratio in

the nanoporous PS mask, in these samples the SiO_2 surface available for implantation is only 25% of the total SiO_2 area. The values obtained for this set of samples are compared with those obtained in the case of the reference samples implanted directly in the SiO_2 film, without the nanoporous polymeric mask. In these samples 100% of the substrate area is exposed to the flux of impinging Si^+ ions during the implantation process. It this worth to note that for the latter set of samples the integral of the Si_2^- signals exhibit a linear dependence on the fluence. This result is quite surprising, in terms of ToF-SIMS analysis, since the excess of silicon introduced in the SiO_2 matrix is very high and severe matrix effects are expected to occur in this range of concentrations, introducing significant deviations from linearity. Nevertheless this linear behavior is observed to survive in a quite broad range of fluencies ranging from $0.3x10^{16}$ to $1.5x10^{16}$ ions/cm^2.

These values are compared with those obtained in the case of the reference samples implanted directly in the SiO_2 film without the nanoporous polymeric mask. It is worth to note that the integrated Si_2^- values of the samples implanted throughout the polymeric mask are significantly lower than the ones obtained on the unmasked samples. These results confirm that a huge amount of the impinging Si^+ ions is efficiently trapped in the polymeric mask and only a fraction of these ions is effectively implanted in the SiO_2 substrate. Moreover it is worth to note that Si_2^- values for the samples implanted throughout the nanoporous PS template correspond to 31% of the values of the same integrals in the case of the implantation performed on the bare SiO_2 sample. These values are in good agreement with the expected fraction of implanted Si^+ ions considering the pore/surface ratio of the nanoporous template. In order to validate this semi-quantitative analysis we implanted Si^+ ions in a slightly different polymeric template exhibiting the same spacing L_0 of the pores but larger pores with diameter $d = 20.7 \pm 0.7$ nm, corresponding

to a pore/surface ratio of 37%. The integrated Si_2^- values for the samples implanted with this nanoporous template are reported in figure 4 for the fluencies $0.75x10^{16}$ and $1.0x10^{16}$ ions/cm^2 respectively. The integrated Si_2- values of these samples correspond to 50% of the values of the same integrals in the case of the implantation performed on the bare SiO_2 sample demonstrating that the amount of Si trapped in the SiO_2 can be finely modulated by changing the Si^+ fluence during implantation and by modifying the dimension of the pores in the mask at the nanometer level.

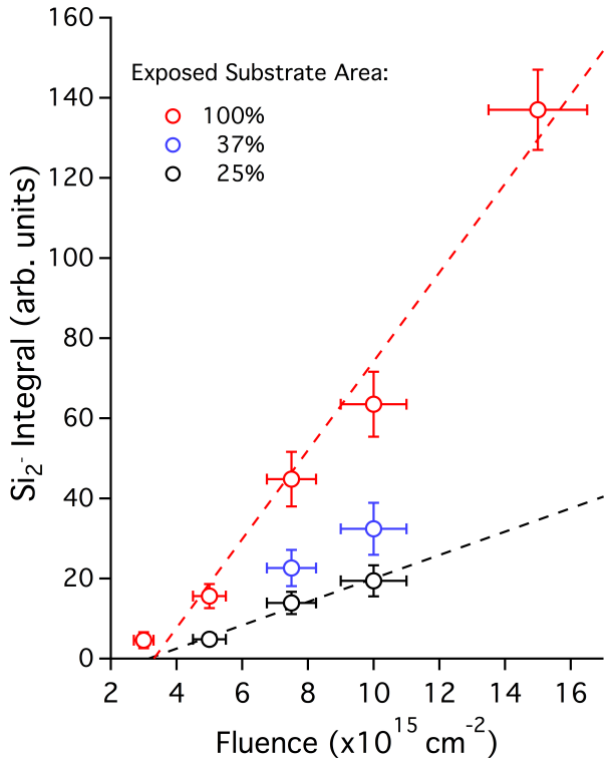

Figure 4. The integrated Si_2^- values of the TOF-SIMS depth profiles are reported as a function of implantation fluencies for the flat samples (red circles). Data are compared with those obtained implanting through the nanoporous PS template (black circles). A different BCP template with larger pores (blue circles) was used to countercheck the capability to control the dose effectively implanted through the polymeric mask.

In summary, ToF-SIMS data demonstrate that there is no significant loss of silicon during implantation throughout the nanoporous polymeric mask. Despite the very thin polymeric film used as a mask, a significative part of the impinging Si^+ ions is efficiently trapped by the

nanoporous PS template, and part is effectively implanted into the oxide. No evidence of shadowing effects due to the presence of the mask is observed in the explored range of fluencies.

3.3. Minimum fluence for Si NPs formation

EFTEM at the plasmon energy of Si was performed in order to get evidence of the localized formation of silicon NPs. With this method, the Si NPs can be imaged directly whatever their crystalline state and orientation. The images can be obtained along two perpendicular directions, plan-view and cross-section. In the obtained images, the NPs appear in white over a dark background that corresponds to the SiO_2 matrix in which the NPs are embedded [31].

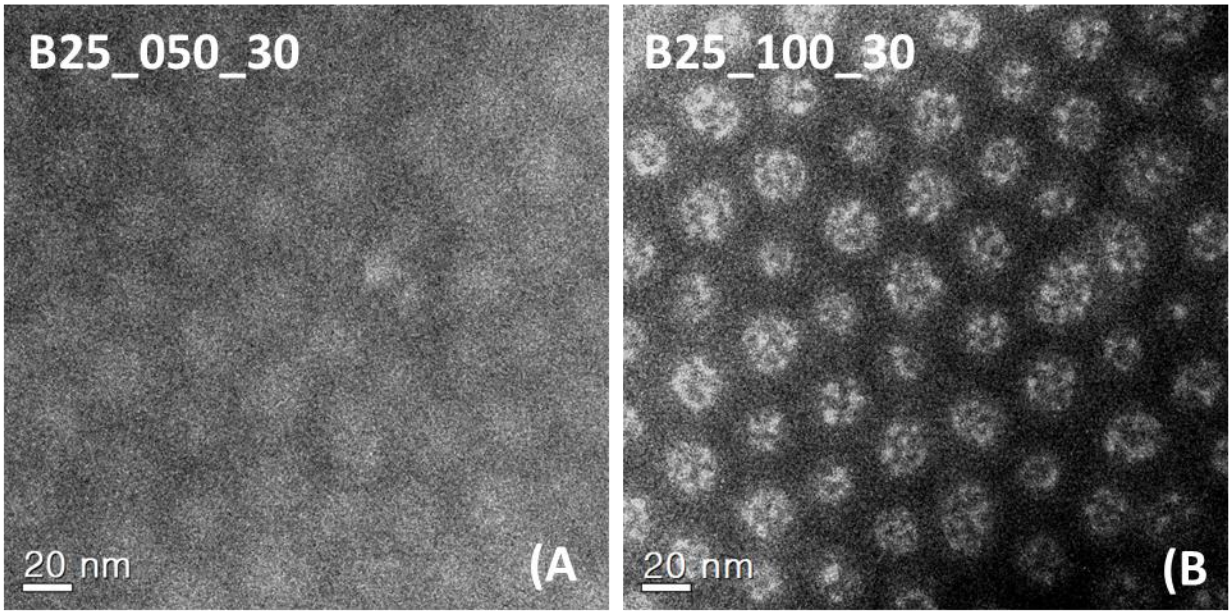

Figure 5. EFTEM images of plan-view samples of the masked SiO_2 thin films after Si^+ ion implantation with 0.5 10^{16} ions/cm^2 (a) and 10^{16} ions/cm^2 (b) followed by thermal annealing.

Plan-view images of the implanted films with the lowest ($0.5x10^{16}$ ions/cm^2) and the highest ($1x10^{16}$ ions/cm^2) Si^+ fluences and annealed at 1050°C for 30 min are shown on figure 5. For the highest fluence, Si NPs are grouped within nanovolumes, with lateral size around 20 nm. These nanovolumes are placed at the nodes of a hexagonal network that mimics the original structure of the nanoporous polymeric mask. The situation is similar for the medium fluence ($0.75x10^{16}$ ions/cm^2) (Figure 6.C) in agreement with data previously reported in the literature [30]. Conversely the EFTEM images depict a different scenario for the lowest fluence, where only diffuse circular domains are seen without any evidence of NPs formation inside these regions. This situation is confirmed from the corresponding cross-sections images where, for the highest fluence (Supplementary data figure 2 (B)), NPs appear aligned forming a plane at nearly 3 nm in depth from the surface of the SiO_2 film and, for the lowest fluence (Supplementary data figure 1 (A)), there is no clear evidence of the presence of silicon nanoparticles. For this last case, the Si^+ fluence can be considered as not high enough to induce the Si supersaturation needed to lead to a phase separation between Si and the SiO_2 matrix and the subsequent formation of the Si NPs.

These results demonstrate that combining a nanoporous BCP template and ULE-IBS, we are able to arrange nanovolumes, at the node of a hexagonal array, with a limited number of Si NPs when the fluence is at least above $0.5x10^{16}$ Si^+ ions/cm². The isolated Si nanoparticles are confined in a single plane at a controlled depth from the sample surface.

3.4. Effects of fluence and annealing duration on the NPs characteristics

To support our investigation, the projected area of the Si NPs and the number of nanoparticles per nanovolume were determined by a numerical treatment of several plan-view images like the ones of figure 6. The grey-level images were binarized to identify the different NPs in the SiO_2 matrix [31]. A population of at least 150 NPs was considered for the treatment of each case. This

statistical method allows a direct measurement of the NPs area, which is more accurate than the one previously proposed in a previous work [30] where the area of the NPs was calculated from the measurements of the length and width of the Si NPs.

Qualitatively, it is observed from figure 6 that Si NPs are larger for the highest Si^+ ion fluence. They appear mainly elongated except for the medium fluence ($0.75x10^{16}$ ions/cm^2) and highest annealing duration (90 min) where they become more circular (Fig.6 E). Quantitatively, the results of the treatment of the images are shown as histograms of frequency of the areas of the Si NPs in figure 7. If we compare the 30 min annealed samples masked (B) and not masked (F), we observe that implanting through the BCP mask induces the formation of a minority population of larger NPs. Nervertheless, a longer annealing duration (90 min) allows to eliminate these large NPs. At the same time, the dispersion in size of the NPs is reduced, which is a favorable trend towards the controlled fabrication of nanometric sized NPs. This trend is more pronounced when decreasing the Si^+ ion fluence. With the aim to fabricate organized NPs of small and same size, it appears clearly that working with a medium fluence is the best option.

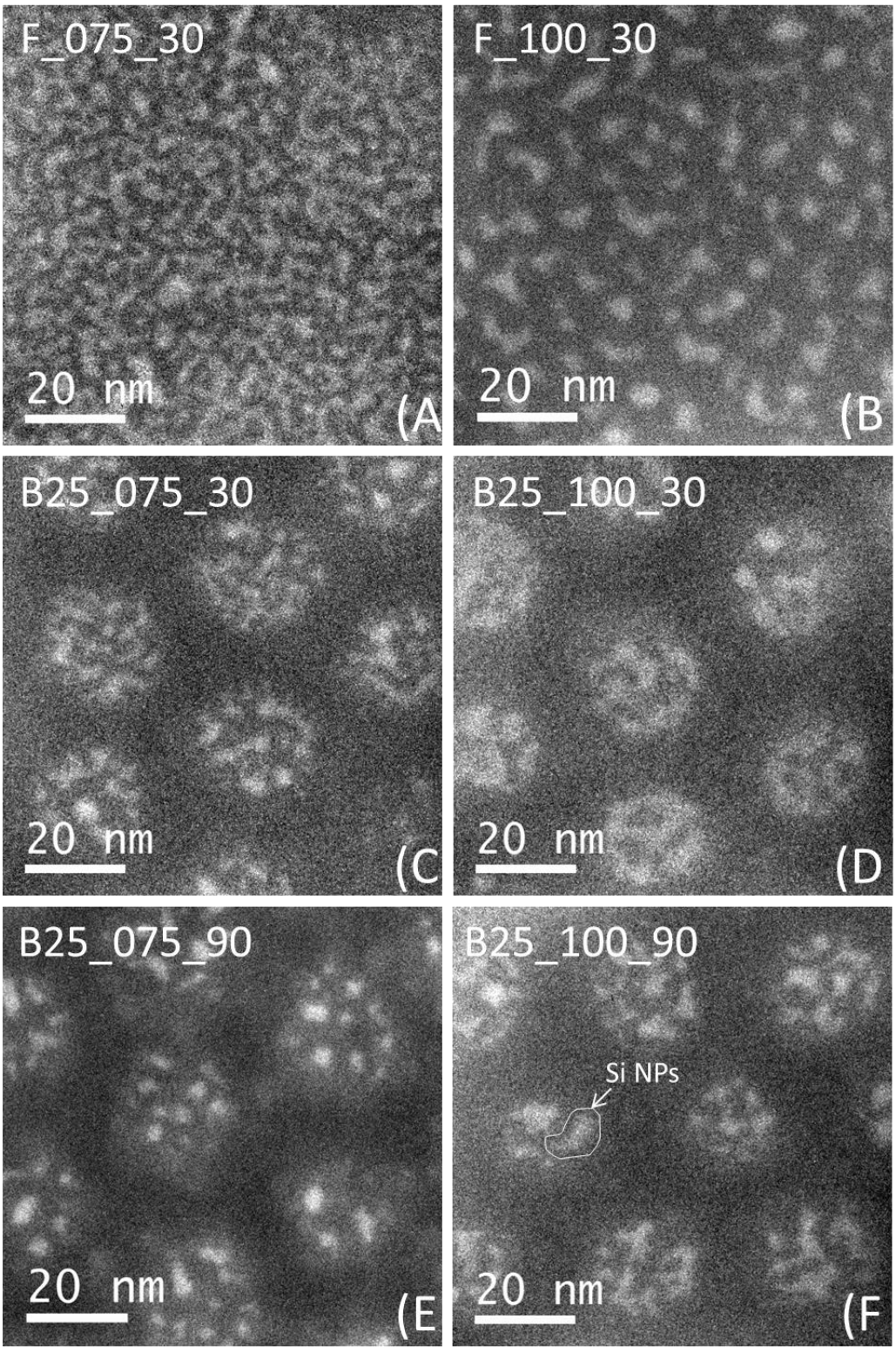

Figure 6. EFTEM images of plan-view TEM lamella obtained from samples implanted with a fluence of (left) 0.75 10^{16} ions/cm^2 and (right) 10^{16} ions/cm^2, without the use of the BCP mask (a, b) and with the BCP mask (c to f). Images (c) and (d) correspond to sample annealed for 30 min and images (e) and (f) to samples annealed for 90 min. On (f), one Si NP is identified with a white contour.

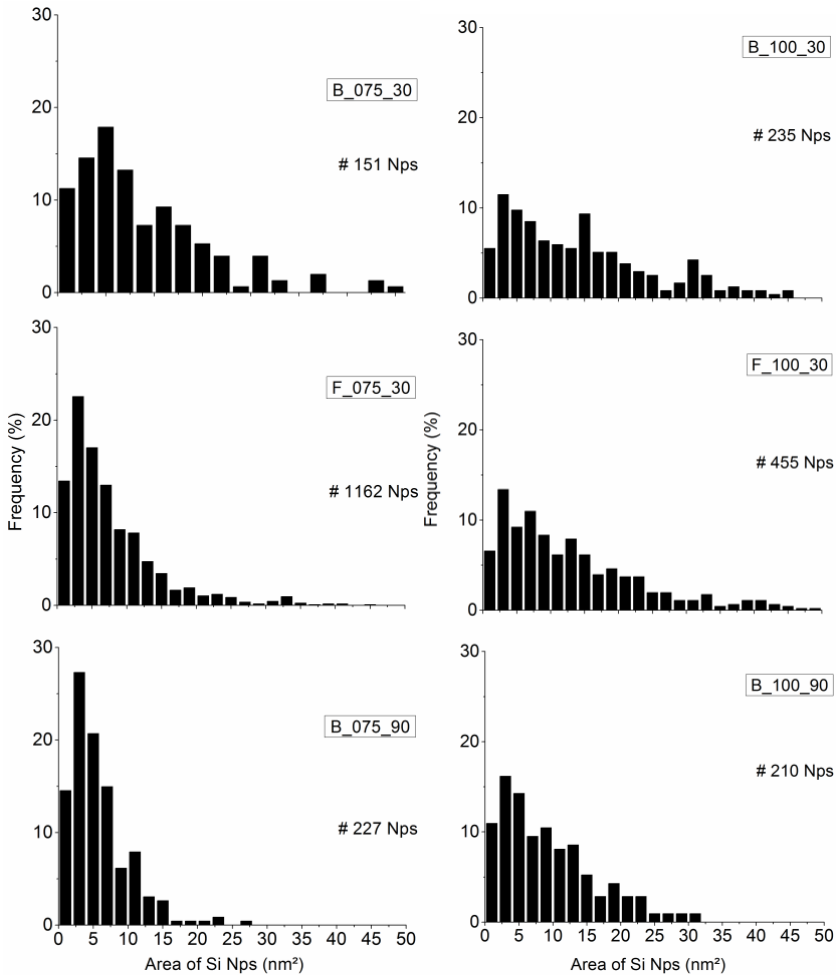

Figure 7. Distribution of area of the Si NPs for each sample**.**

For a further discussion, the data of the histograms for the medium fluence are displayed in a different way in figure 8. The Si NPs projected areas are gathered and distributed among 3 ranges named “small” for areas lower than 10 nm^2, “medium” for areas in the range [10-20] nm^2 and “large” for areas higher than 20 nm^2. This classification allows highlighting more quantitatively the main changes due to the modifications of the fabrication parameters. If we concentrate on the small NPs range, the 30 min annealing duration allows to fabricate a maximum level of only 65% of small NPs whereas a 90 min annealing duration opens the possibility to reach a value of 85%.

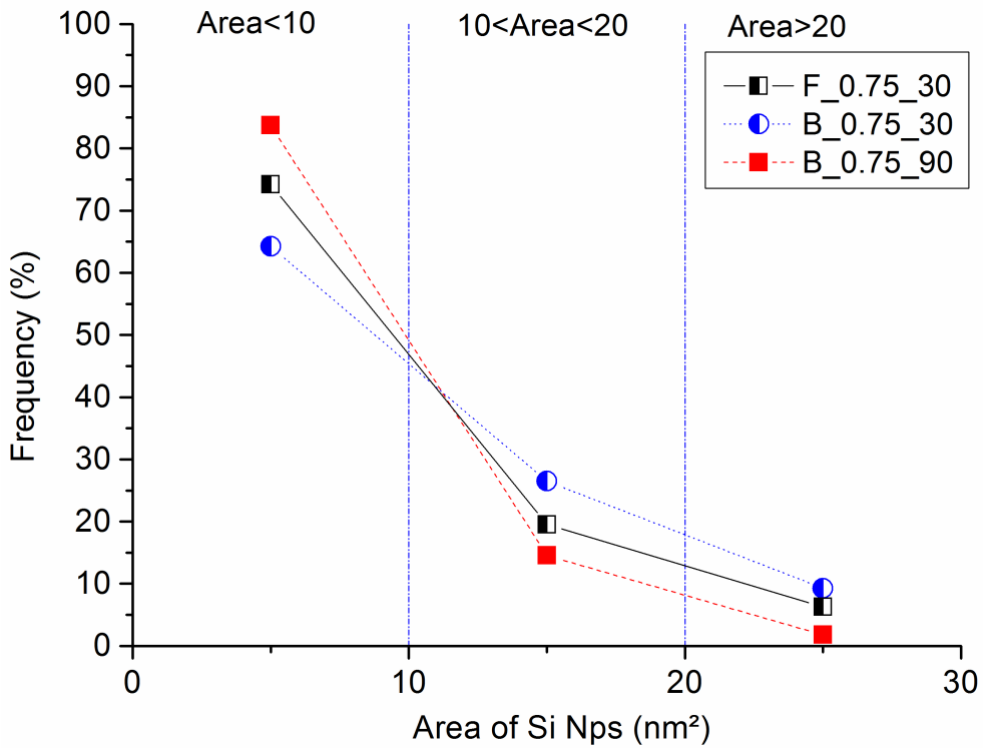

Figure 8. Si NPs population divided in 3 categories of area: "small" area<10 nm^2, "medium" area [10-20] nm^2 and "large" area>20 nm^2.

Figure 9 illustrates the average values of the Si NPs areas and the corresponding average number of NPs per nanovolume as a function of the fabrication parameters. The ordering of the fabrication parameters was selected in order to better evidence the previously discussed trends in the NPs characteristics. The mean size of the NPs can be decreased from 16 nm^2 to 6 nm^2 by increasing the annealing duration and decreasing the fluence. This behavior is opposite to the increase of the corresponding number of NPs per nanovolume from 6 to 10. Furthermore, it is noticeable that for the 0.75 10^{16} ions/cm^2 fluence, increasing the annealing duration from 30 to 90 min has no significant effect on the number of Si NPs per nanovolume but this number

remains too high for the targeted applications. Therefore, to manipulate at the same time the size (low dispersion of nanometer sized nanoparticles) and the number (towards unity) of Si NPs per nanovolume, new strategies have to be investigated.

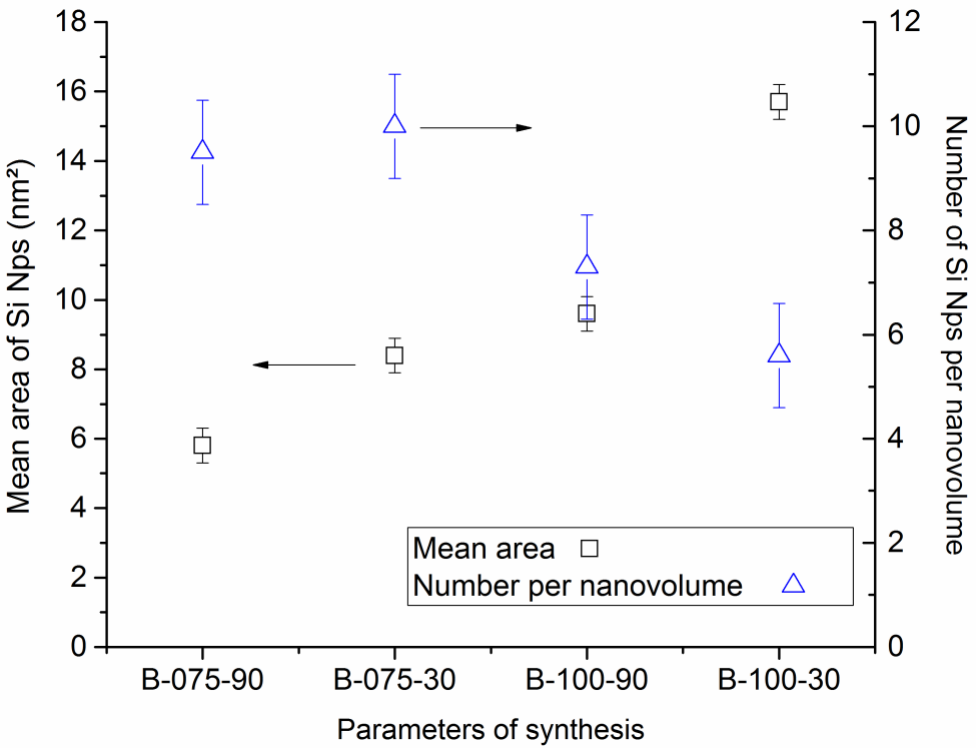

Figure 9. Mean area and number per nanovolume of Si NPs as function of samples parameters. The ordering of the fabrication parameters was selected in order to better evidence the trends in the NPs characteristics.

4. Discussion

On the basis of the kinetic Monte Carlo simulations of Müller et al. [36] dedicated to the Si NPs formation by phase separation during annealing in the context of ion beam synthesis in thin SiO_2 films, we tried to get a picture about the mechanisms of formation and evolution during annealing of the NPs we fabricated. From figure 6, it appears clearly that the NPs synthesized by

Si^+ ion implantation without any polymeric mask are mostly elongated. The occurrence of Si NPs with this peculiar shape is well described according to Müller's work by a phase separation between Si and SiO_2 through a «spinodal decomposition» mechanism. If implantation occurs throughout the BCP mask, the same mechanism seems to be concerned being enhanced by the confinement of the Si excess into defined nanovolumes. Indeed, for an annealing duration of 30 min, confinement of the NPs into nanovolumes induces the formation of NPs in the "medium" and "large" ranges at the expense of the "small" one. This result supports the idea that the implanted Si supersaturation is somehow increased within the nanovolumes, maybe due to peculiar effects occurring at the interface between the Si rich nanovolumes and the surrounding matrix. Experimental data clearly indicate that this condition is favorable for spinodal decomposition. According to Müller's study, a very long annealing duration is necessary to make the elongated NPs evolve into spherical ones. Indeed, with time, NPs dissolve by Si loss to the Si/SiO_2 interface due to interfacial energy minimization of the Si/SiO_2 mixture [36].

Actually the analysis of the samples annealed at 1050°C for 90 min indicate a clear evolution of the Si NP population, with a significant increase in the fraction of small Si NPs. This result suggests the possibility to further improve the control on the size of the Si NPs by finely tuning the annealing parameters. As discussed in [20], annealing under oxidizing atmosphere is an efficient way to consume the NPs and could represent an alternative strategy to reduce and homogenize their size.

However in order to achieve the final goal of organizing individual Si NPs in well precise locations with nanometer accuracy, the use of BCP masks with smaller pore diameters is necessarily required. Actually the size of the nanopores can be finely tuned by proper selection of the PS-b-PMMA BCP. By adjusting the molecular weight of the PS-b-PMMA block

copolymer it is possible to adjust the average pore diameter down to d =12 nm [37,38]. In this way it would be possible to further reduce the number of the Si NPs formed in each single pore getting close to the limit of one isolated nanoparticle per pore. The registration of the BCP periodic microdomains in predefined locations of the substrate is a prerequisite for the in-plane positioning of the Si NPs. Several methods were proposed to register the BCP microdomains to the substrate surface, including chemical patterning of the substrate [39,40] as well as soft [41,42] and hard graphoepitaxy [43,44]. The latter approach is based on the topographically sectoring of a surface with standard lithographic processes. In this way addressable arrays of cylindrical elements can be registered with the underlying substrate improving at the same time the accuracy in their positioning on the sample surface [45–48]. The combination of these top-down and bottom up approaches is in principle perfectly compatible with conventional semiconductor technology and would represent a viable approach to control the placement of Si NPs in a thin SiO_2 layer with nanometer accuracy in all the 3 spatial dimensions.

5. Conclusion

In this work we coupled ULE-IBS with thermal annealing and BCP nanopatterning. The result is the spatial organization of the silicon NPs in a 2D hexagonal array at a controlled depth of thin SiO_2 films.

The fabrication parameters were varied and the results were investigated by TOF-SIMS at large scale and EFTEM for local studies.

With the following parameters investigated, i.e. BCP mask with 17 nm pores and 1keV, $0.75x10^{16}$ or $1x10^{16}$ Si^+ ions/cm² implantation parameters, the mean size of NPs can be

modulated in the range from 6 to 16 nm² with a corresponding mean number of NPs per nanovolume being between 10 and 5.6 respectively.

The discussion compared these results with published kinetic Monte Carlo simulations [36] and previous works[20]. In particular, the effect of the confinement due to implantation through the BCP mask, of the fluence and of the annealing duration on the size and number per nanovolume of Si NPs have been considered here.

Based on these results several routes are opened toward new synthesis strategies able to organize single Si nanocrystals such as longer annealing times within neutral or oxidizing atmosphere like N_2+O_2 mixed gas [20] coupled with BCP masks were pore diameters are smaller, in the 10 nm[25] range. In addition this fabrication method is quite generic and could be applied to other couples of ions and substrate.

Acknowledgements

This research was supported by the ERANET PLUS "NanoSci-E+" consortium through the NANO-BLOCK (NANO-device fabrication using BLOCK copolymer based technology) project.

References

[1] Hoefflinger B 2011 ITRS: The International Technology Roadmap for Semiconductors *Chips 2020* The Frontiers Collection ed B Hoefflinger (Springer Berlin Heidelberg) pp 161–74

[2] Black C T 2007 Polymer Self-Assembly as a Novel Extension to Optical Lithography *ACS Nano* **1** 147–50

[3] Prati E 2013 Single electron effects in silicon quantum devices *J. Nanoparticle Res.* **15** 1–10

[4] Shin K, Leach K A, Goldbach J T, Kim D H, Jho J Y, Tuominen M, Hawker C J and Russell T P 2002 A Simple Route to Metal Nanodots and Nanoporous Metal Films *Nano Lett.* **2** 933–6

[5] Jeong S-J, Xia G, Kim B H, Shin D O, Kwon S-H, Kang S-W and Kim S O 2008 Universal Block Copolymer Lithography for Metals, Semiconductors, Ceramics, and Polymers *Adv. Mater.* **20** 1898–904

[6] Bonafos C 2004 Manipulation of two-dimensional arrays of Si nanocrystals embedded in thin SiO_2 layers by low energy ion implantation *J. Appl. Phys.* **95** 5696

[7] Normand P *et al.* 2004 Nanocrystals manufacturing by ultra-low-energy ion-beam-synthesis for non-volatile memory applications *Nucl. Instrum. Methods* **216** 228–38

[8] Tiwari S, Rana F, Hanafi H, Hartstein A, Crabbé E F and Chan K 1996 A silicon nanocrystals based memory *Appl. Phys. Lett.* **68** 1377

[9] Maeda T, Suzuki E, Sakata I, Yamanaka M and Ishii K 1999 Electrical properties of Si nanocrystals embedded in an ultrathin oxide *Nanotechnology* **10** 127–31

[10] Ostraat M L, De Blauwe J W, Green M L, Bell L D, Brongersma M L, Casperson J, Flagan R C and Atwater H A 2001 Synthesis and characterization of aerosol silicon nanocrystal nonvolatile floating-gate memory devices *Appl. Phys. Lett.* **79** 433–5

[11] Zacharias M, Heitmann J, Scholz R, Kahler U, Schmidt M and Bläsing J 2002 Size-controlled highly luminescent silicon nanocrystals: A SiO/SiO2 superlattice approach *Appl. Phys. Lett.* **80** 661–3

[12] Steimle R F *et al.* 2007 Silicon nanocrystal non-volatile memory for embedded memory scaling *Microelectron. Reliab.* **47** 585–92

[13] Lai S K 2008 Flash memories: Successes and challenges *IBM J. Res. Dev.* **52** 529–35

[14] Khriachtchev L 2008 *Silicon Nanophotonics: Basic Principles, Current Status and Perspectives* (Singapore : Hackensack, NJ: Pan Stanford)

[15] Conibeer G *et al.* 2006 Silicon nanostructures for third generation photovoltaic solar cells *Thin Solid Films* **511–512** 654–62

[16] Koshida N 2008 *Device Applications of Silicon Nanocrystals and Nanostructures* (Springer)

[17] Carles R, Farcau C, Bonafos C, Benassayag G, Bayle M, Benzo P, Groenen J and Zwick A 2011 Three Dimensional Design of Silver Nanoparticle Assemblies Embedded in Dielectrics for Raman Spectroscopy Enhancement and Dark-Field Imaging *ACS Nano* **5** 8774–82

[18] Assayag G B, Bonafos C, Carrada M, Claverie A, Normand P and Tsoukalas D 2003 Transmission electron microscopy measurements of the injection distances in nanocrystal-based memories *Appl. Phys. Lett.* **82** 200–2

[19] Carrada M, Cherkashin N, Bonafos C, Benassayag G, Chassaing D, Normand P, Tsoukalas D, Soncini V and Claverie A 2003 Effect of ion energy and dose on the positioning of 2D-arrays of Si nanocrystals ion beam synthesised in thin SiO2 layers *Mater. Sci. Eng. B* **101** 204–7

[20] Bonafos C, Coffin H, Schamm S, Cherkashin N, Ben Assayag G, Dimitrakis P, Normand P, Carrada M, Paillard V and Claverie A 2005 Si nanocrystals by ultra-low-energy ion beam-synthesis for non-volatile memory applications *Solid-State Electron.* **49** 1734–44

[21] Grisolia J, Dumas C, Ben Assayag G, Bonafos C, Schamm S, Arbouet A, Paillard V, van den Boogaart M A F, Brugger J and Normand P 2008 Silicon nanoparticles synthesized in SiO2 pockets by stencil-masked low energy ion implantation and thermal annealing *Superlattices Microstruct.* **44** 395–401

[22] Pease R F and Chou S Y 2008 Lithography and Other Patterning Techniques for Future Electronics *Proc. IEEE* **96** 248–70

[23] Herr D J C 2011 Directed block copolymer self-assembly for nanoelectronics fabrication *J. Mater. Res.* **26** 122–39

[24] Perego M and Seguini G 2016 Self-assembly strategies for the synthesis of functional nanostructured materials *Nuovo Cimento Riv. Ser.* **39** 1

[25] Son J G, Chang J-B, Berggren K K and Ross C A 2011 Assembly of Sub-10-nm Block Copolymer Patterns with Mixed Morphology and Period Using Electron Irradiation and Solvent Annealing *Nano Lett* **11** 5079–84

[26] Bates F S and Fredrickson G H 1999 Block Copolymers—Designer Soft Materials *Phys. Today* **52** 32–8

[27] Andreozzi A, Poliani E, Seguini G and Perego M 2011 The effect of random copolymer on the characteristic dimensions of cylinder-forming PS-*b*-PMMA thin films *Nanotechnology* **22** 185304

[28] Farrell R A, Petkov N, Morris M A and Holmes J D 2010 Self-assembled templates for the generation of arrays of 1-dimensional nanostructures: From molecules to devices *J. Colloid Interface Sci.* **349** 449–72

[29] Andreozzi A, Lamagna L, Seguini G, Fanciulli M, Schamm-Chardon S, Castro C and Perego M 2011 The fabrication of tunable nanoporous oxide surfaces by block copolymer lithography and atomic layer deposition *Nanotechnology* **22** 335303

[30] Castro C, Schamm-Chardon S, Pecassou B, Andreozzi A, Seguini G, Perego M and BenAssayag G 2013 In-plane organization of silicon nanocrystals embedded in SiO2 thin films *Nanotechnology* **24** 075302

[31] Schamm S, Bonafos C, Coffin H, Cherkashin N, Carrada M, Ben Assayag G, Claverie A, Tencé M and Colliex C 2008 Imaging Si nanoparticles embedded in SiO2 layers by (S)TEM-EELS *Ultramicroscopy* **108** 346–57

[32] Ferrari S, Perego M and Fanciulli M 2003 Quantitative depth profiling at silicon/silicon oxide interfaces by means of Cs+ sputtering in negative mode by ToF-SIMS: a full spectrum approach *Appl. Surf. Sci.* **203–204** 52–5

[33] Perego M, Ferrari S, Spiga S, Bonera E, Fanciulli M and Soncini V 2003 Time of flight secondary ion mass spectrometry study of silicon nanoclusters embedded in thin silicon oxide layers *Appl. Phys. Lett.* **82** 121–3

[34] Perego M, Ferrari S, Fanciulli M, Ben Assayag G, Bonafos C, Carrada M and Claverie A 2004 Characterization of silicon nanocrystals embedded in thin oxide layers by TOF-SIMS *Appl. Surf. Sci.* **231–232** 813–6

[35] Perego M, Ferrari S, Fanciulli M, Ben Assayag G, Bonafos C, Carrada M and Claverie A 2004 Detection and characterization of silicon nanocrystals embedded in thin oxide layers *J. Appl. Phys.* **95** 257–62

[36] Müller T, Heinig K-H and Möller W 2002 Size and location control of Si nanocrystals at ion beam synthesis in thin SiO2 films *Appl. Phys. Lett.* **81** 3049–51

[37] Seguini G *et al.* 2014 Thermally induced self-assembly of cylindrical nanodomains in low molecular weight PS-*b*-PMMA thin films *Nanotechnology* **25** 045301

[38] Ferrarese Lupi F, Giammaria T J, Seguini G, Vita F, Francescangeli O, Sparnacci K, Antonioli D, Gianotti V, Laus M and Perego M 2014 Fine tuning of lithographic masks through thin films of PS-b-PMMA with different molar mass by rapid thermal processing *ACS Appl. Mater. Interfaces* **6** 7180–8

[39] Ouk Kim S, Solak H H, Stoykovich M P, Ferrier N J, de Pablo J J and Nealey P F 2003 Epitaxial self-assembly of block copolymers on lithographically defined nanopatterned substrates *Nature* **424** 411–4

[40] Liu G, Detcheverry F, Ramírez-Hernández A, Yoshida H, Tada Y, de Pablo J J and Nealey P F 2012 Nonbulk Complex Structures in Thin Films of Symmetric Block Copolymers on Chemically Nanopatterned Surfaces *Macromolecules* **45** 3986–92

[41] Jeong S-J, Kim J E, Moon H-S, Kim B H, Kim S M, Kim J B and Kim S O 2009 Soft Graphoepitaxy of Block Copolymer Assembly with Disposable Photoresist Confinement *Nano Lett.* **9** 2300–5

[42] Jeong S-J and Kim S O 2011 Ultralarge-area block copolymer lithography via soft graphoepitaxy *J. Mater. Chem.* **21** 5856–9

[43] Park S-M, Rettner C T, Pitera J W and Kim H-C 2009 Directed Self-Assembly of Lamellar Microdomains of Block Copolymers Using Topographic Guiding Patterns *Macromolecules* **42** 5895–9

[44] Sundrani D, Darling S B and Sibener S J 2004 Guiding Polymers to Perfection: Macroscopic Alignment of Nanoscale Domains *Nano Lett.* **4** 273–6

[45] Cheng J Y, Mayes A M and Ross C A 2004 Nanostructure engineering by templated self-assembly of block copolymers *Nat. Mater.* **3** 823–8

[46] Tong Q and Sibener S J 2013 Visualization of Individual Defect Mobility and Annihilation within Cylinder-Forming Diblock Copolymer Thin Films on Nanopatterned Substrates *Macromolecules* **46** 8538–44

[47] Perego M, Andreozzi A, Vellei A, Lupi F F and Seguini G 2013 Collective behavior of block copolymer thin films within periodic topographical structures *Nanotechnology* **24** 245301

[48] Ferrarese Lupi F, Giammaria T, Seguini G, Laus M, Enrico E, De Leo M, Boarino L, Ober C and Perego M 2014 Thermally induced orientational flipping of cylindrical phase diblock copolymers *J. Mater. Chem. C* **2** 2175–82